sciendo

CrossMark

Moroccan J. of Pure and Appl. Anal. (MJPAA)
Volume 9(1), 2023, Pages 141–153
ISSN: Online 2351-8227 - Print 2605-6364
DOI: 10.2478/mjpaa-2023-0010

Parameters identification for a nonlinear partial differential equation in image denoising

A. EL MOURABIT[1]

Abstract. In this work and in the context of PDE constrained optimization problems, we are interested in identification of a parameter in the diffusion equation proposed in [1]. We propose to identify this parameter automatically by a gradient descent algorithm to improve the restoration of a noisy image. Finally, we give numerical results to illustrate the performance of the automatic selection of this parameter and compare our numerical results with other image denoising approaches or algorithms.

Mathematics Subject Classification (2020). MSC 45H30, MSC 35K10.
Key words and phrases. Optimization problems, Diffusion equation, Parameters identification.

1. Introduction

Image processing has great importance in a number of fields, for example: photography, digital cinema, astronomy and medicine, ... Therefore, it has been the subject of attention of a number of researchers. One of the fundamental problems in the field of image processing is the reduction of noise (or denoising) of images [3, 17]. Given an image function u_0 defined on Ω, with $\Omega \subset \mathbb{R}^2$ an open and bounded domain, the problem is to start from an observation u_0, restore or reconstruct a real image u, this is an important task in image processing, to improve the quality of the image or to obtain both a reduction of the noise and the preservation of important features of the image.

Received : June 16, 2022 - Accepted : October 27, 2022.
©The Author(s) 2023. This article is published with open access by Sidi Mohamed Ben Abdallah University.
[1] *Ecole Supérieure de Technologie-Essaouira B.P 383 Essaouira Université Cadi Ayyad.*
e-mail : elmourabitabdelmajid@gmail.com .

In denouncing problems, u is the solution to an ill-posed reverse problem that is presented as follows

$$u_0(i,j) = u(i,j) + \eta(i,j), \tag{1.1}$$

where $u_0(i,j)$ is noisy image at pixel (i,j) and $\eta(i,j)$ is an additive Gaussian noise at pixel (i,j) with standard deviation σ_n [16], which can be estimated in practical applications by various methods. There are many denoising models based on a variational approach [20, 12]. For exemple, the work of Rudin, Osher and Fatemi [20], regularization by the functions of (TV) has received considerable attention in the treatment of image and signal. Thus, the (TV) model is effective in reducing image noise and preserving the edge, but it suffers from the staircase effect. For this reason, a lot of work has been done to improve the TV model to reduce the staircase effect, e.g. Total Generalized Variation (TGV) model [5], the high-order TV methods [21, 6] and the fractional TV model [25].
The noise can be grouped into two classes:

- Noise that depends on the image data,
- Independent noise (we speak of random noise).

The image noise is like a random field, because of its high frequency, we keep to characterize the first order (no correlation between pixels) and sometimes the second order (correlation between pixels). To compute the denoised image $\widehat{u}$, there are denoising methods use image priors and minimize an energy function $\mathcal{J}$, such that we obtain a function $\mathcal{J}$ from a noisy image u_0, then a low number corresponds to a noise-free image by a matching procedure. Finally, by minimizing E to obtain a denoised image $\widehat{u}$:

$$\widehat{u} \in \arg\min_u \mathcal{J}(u). \tag{1.2}$$

To jointly reconstruct u and u_0, we rely on the maximum a posteriori (MAP) which consists in maximizing the posterior estimate $\mathcal{P}(u|u_0)$ of u as follows

$$\widehat{u} = \arg\max_u \mathcal{P}(u|u_0) = \arg\max_u \frac{\mathcal{P}(u_0|u)\mathcal{P}(u)}{\mathcal{P}(u_0)}, \tag{1.3}$$

then

$$\widehat{u} = \arg\max_u \log \mathcal{P}(u_0|u) + \log \mathcal{P}(u), \tag{1.4}$$

with $\mathcal{P}(u_0|u)$ is a likelihood function of u, and $\mathcal{P}(u)$ is the prior image.
In the case of additive white Gaussian noise with standard deviation σ_n, we can formulate the objective function as

$$\widehat{u} = \arg\min_u \frac{1}{2}||u - u_0||^2_{L^2(\Omega)} + \alpha\mathcal{R}(u) \tag{1.5}$$

where Ω is a bounded open subset of $\mathbb{R}^2$, $\mathcal{R}$ denotes a regularization term and α is a non-negative regularization parameter.
Note also that $||u - u_0||^2_{L^2(\Omega)}$ is a data fidelity term that is the difference between the original and noisy images and determining the appropriate image prior $\mathcal{R}(u)$ is a proposed key to variational denoising methods. With varying degrees of success, various functions have been proposed in the literature.

Perona and Malik (PM)(see [19]), they take $\mathcal{R}(u) = \exp\left(-\left[\frac{|\nabla u|}{\kappa}\right]^2\right)$ and proposed a reaction-diffusion equation with anisotropic diffusion

$$\frac{\partial u}{\partial t} = div[D(|\nabla u|)\nabla u] = D(|\nabla u|)\triangle u + \triangle u D(|\nabla u|).\nabla u, \tag{1.6}$$

with $D(|\nabla u|)$ denotes the diffusion coefficient and satisfies the following conditions:

$$\lim_{|\nabla u|\to 0} D(|\nabla u|) = 1 \text{ and } \lim_{|\nabla u|\to\infty} D(|\nabla u|) = 0, \tag{1.7}$$

the model of (PM) able to in enhancing the edges, but the staircase effect is obvious.

In [20] Rudin, Osher and Fatemi consider $\mathcal{R}(u) = TV(u)$ and proposed to minimize the following function

$$\widehat{u} = \arg\min_u \frac{1}{2}||u - u_0||^2_{L^2(\Omega)} + \alpha TV(u) \tag{1.8}$$

where

$$TV(u) = \int_\Omega |Du|dx = \sup\left\{\int_\Omega u div\varphi dx,\ \varphi \in C^1(\Omega, \mathbb{R}) \text{ and } ||\varphi||_\infty \leqslant 1\right\},$$

but this approach strengthens the piecewise constant structures more than the smooth structures, which gives a staircase effect. In order to reduce this effect and improve the image quality, the authors in [1], has proposed the following equation

$$\begin{cases} \dfrac{\partial u}{\partial t} - div\left(\dfrac{\log^\gamma(1+|\nabla u|)}{|\nabla u|}\nabla u\right) + \lambda u - u_0 = 0 \quad in \quad \Omega\times(0,T), \\ \left\langle \dfrac{\log^\gamma(1+|\nabla u|)}{|\nabla u|}\nabla u, n\right\rangle = 0 \quad \text{in } \partial\Omega\times(0,T), \\ u(x,0) = u_0 \quad \text{in } \Omega. \end{cases} \tag{1.9}$$

Also, they yield a result of existence for solutions of (1.9) in a general framework.

Our objective is to analyze and implement a bilevel optimization framework to automatically select the regularization parameter λ setting in the following image reconstruction issue:

$$\min_{\lambda\in\mathcal{U}_{ad}} \mathcal{J}(\lambda), \tag{1.10}$$

where

$$\mathcal{J}(\lambda) = \frac{1}{2}\int_\Omega |u(T,x) - u_0(x)|^2 dx + \frac{\alpha}{2}\int_\Omega |\lambda(x)|^2 dx,$$

subject to

$$(\mathcal{SE})\begin{cases} \dfrac{\partial u}{\partial t} - div\left(\dfrac{\log^\gamma(1+|\nabla u|)}{|\nabla u|}\nabla u\right) + \lambda(u - u_0) = 0 \quad in \ \ \Omega\times(0,T), \\ \left\langle \dfrac{\log^\gamma(1+|\nabla u|)}{|\nabla u|}\nabla u, n\right\rangle = 0 \quad in \ \ \partial\Omega\times(0,T), \\ u(x,0) = u_0 \quad in \ \ \Omega, \end{cases} \tag{1.11}$$

where u_0 represents the input image assumed to be a bounded function, α a positive constant, γ is the weighting parameter to be estimated in (1.10) and $\mathcal{U}_{ad}$ is the set of admissible functions defined by

$$\mathcal{U}_{ad} = \{\lambda \in L^2(\Omega) : \lambda_a \leqslant \lambda(x) \leqslant \lambda_b \ \ a.e\ in\ \Omega\}, \tag{1.12}$$

where λ_a, $\lambda_b \in \mathbb{R}$ with $0 < \lambda_a < \lambda_b$.
This paper is structured as follows: the existence of a solution for the optimization problem is given in Section 2. Finally, in Section 3 presents the suggested Gradient descent algorithm and the benefits of the proposed method by using comparative experiments with some approaches denoising methods.

2. Existence of solution for the optimization problem

In the sequel we denote by $A(t) = tlog^{\gamma}(1+t), t > 0$.

Proposition 2.1. *Let $(\lambda_k)_k$ be a sequence from $\mathcal{U}_{ad}$ that converges in $L^2(\Omega)$ to $\overline{\lambda} \in \mathcal{U}_{ad}$ and $u_k \equiv u(\lambda_k)$ solution of (1.11), $\forall k \in \mathbb{N}$, then*

1- There exists a subsequence $(u_k)_k$ which converges a.e. to $\overline{u}$ solution of (1.11).
2- The cost functional $\mathcal{J}$ is weakly lower semicontinuous (w.l.s.c.) and satisfies

$$\mathcal{J}(\overline{\lambda}) \leqslant \liminf_{k\to\infty} \mathcal{J}(\lambda_k).$$

Proof. 1- Let's $(\lambda_k)_k$ be a sequence of $\mathcal{U}_{ad}$ and u_k solution of (1.11) related to λ_k, then we have

$$\left\langle \frac{\partial u_k}{\partial t}, \phi \right\rangle_{W^{-1,x}L_{\overline{A}}(Q)+L^2(Q),W^{1,x}L_A(Q)\cap L^2(Q)} + \int_Q a(\gamma, \nabla u_k)\nabla\phi dxdt + \int_Q \lambda_k(u_k - u_0)\phi dxdt = 0, \tag{2.1}$$

for all $\phi \in W^{1,x}L_A(Q) \cap L^2(Q)$ and where $a(\gamma, \nabla u_k) = \dfrac{\log^{\gamma}(1+|\nabla u_k|)}{|\nabla u_k|}\nabla u_k$.

Since $\mathcal{J}$ is coercive in $L^2(\Omega)$; ($\mathcal{J}(\lambda) > \alpha||\lambda||_{L^2(\Omega)}$, with $\alpha > 0$), then $(\lambda_k)_k$ is bounded in $L^2(\Omega)$. Moreover, we have $L^2(\Omega)$ is reflexive so we can extract a subsequence noted again $(\lambda_k)_k$ which converges weakly to $\overline{\lambda}$ in $L^2(\Omega)$

$$\lambda_k \rightharpoonup \overline{\lambda} \ \text{ in } \ L^2(\Omega) \ \text{ and } \ \overline{\lambda} \in \mathcal{U}_{ad}. \tag{2.2}$$

Let $t \in (0, T)$ and choose $\phi = u_k(t)$ as test function in the variational formulation (2.1), we get:

$$\frac{1}{2}\int_\Omega u_k^2(x,t)dx - \frac{1}{2}\int_\Omega u_0^2(x)dx + \int_0^t\int_\Omega \log^{\gamma}(1+|\nabla u_k|)|\nabla u_k|dxdt + \int_0^t\int_\Omega \lambda_k u_k^2(x,t)dxdt$$
$$= \int_0^t\int_\Omega \lambda_k u_k(x,t)u_0(x)dxdt,$$

using the Young's inequality and the fact that $\lambda_k \in \mathcal{U}_{ad}$, we have

$$\frac{1}{2}\int_\Omega u_k^2(t)dx - \frac{1}{2}\int_\Omega u_0^2 dx + \int_0^t\int_\Omega \log^{\gamma}(1+|\nabla u_k|)|\nabla u|dx + \lambda_a\int_0^t\int_\Omega u_k^2(x,t)dxdt$$
$$\leqslant \frac{\lambda_b}{2}\int_0^t\int_\Omega u_k^2(x,t)dxdt + \frac{\lambda_b}{2}\int_0^t\int_\Omega u_0(x)^2 dxdt,$$

then

$$\int_\Omega u_k^2(x,t)dx \leqslant (T\lambda_b + 1)\int_\Omega u_0^2(x)dx + \lambda_b \int_0^t \int_\Omega u_k^2(x,t)dxdt. \tag{2.3}$$

Using Gronwall inequality, we get

$$\int_\Omega u_k^2(x,t)dx \leqslant \left((T\lambda_b + 1)\int_\Omega u_0^2(x)dx\right)\exp(t\lambda_b) \quad \forall t \in (0,T), \tag{2.4}$$

this implies that

$$\int_\Omega u_k^2(x,t)dx \leqslant C, \tag{2.5}$$

for some constant $C > 0$ depending only on T and λ_b. Then $||u_k||_{L^\infty(0,T;L^2(\Omega))} \leqslant C$.
On the other hand

$$\int_0^t \int_\Omega A(|u_k|)dx + \int_0^t \int_\Omega A(|\nabla u_k|)dx \leqslant C, \tag{2.6}$$

Consequently $(u_k)_k$ is bounded in $W^{1,x}L_A(Q) \cap L^2(Q)$ and $\dfrac{\partial u_k}{\partial t}$ is bounded in $W^{-1}L_{\overline{A}}(Q) + L^2(Q)$.
Arguing as in [9, 10] (see proof of Theorem 3.1) we deduce (for a subsequence) that

$$u_k \to \overline{u} \ \ a.e \ \ in \ \ Q. \tag{2.7}$$

and

$$\nabla u_k \longrightarrow \nabla \overline{u} \quad a.e \ \ in \ \ Q, \tag{2.8}$$

and consequently as it is done in [1]

$$u_k \to \overline{u} \ \ in \ \ C([0,T], L^2(\Omega)) \tag{2.9}$$

The passage to the limit in (2.1) is straightforward by adapting again the lines of [1].
2- Show that the cost functional $\mathcal{J}$ satisfies

$$\mathcal{J}(\overline{\lambda}) \leqslant \liminf_{k\to\infty} \mathcal{J}(\lambda_k). \tag{2.10}$$

we have

$$\begin{aligned}
\mathcal{J}(\overline{\lambda}) &= \frac{1}{2}\int_\Omega |\overline{u}(T,x) - u_0(x)|^2 dx + \alpha \int_\Omega |\overline{\lambda}(x)|^2 dx \\
&\leqslant \liminf_{k\longrightarrow+\infty} \frac{1}{2}\int_\Omega |u_k(T,x) - u_0(x)|^2 dx + \liminf_{k\longrightarrow+\infty} \alpha \int_\Omega |\lambda_k(x)|^2 dx \\
&\leqslant \liminf_{k\longrightarrow+\infty} (\frac{1}{2}\int_\Omega |u_k(T,x) - u_0(x)|^2 dx + \alpha \int_\Omega |\lambda_k(x)|^2 dx) \\
&\leqslant \liminf_{k\longrightarrow+\infty} \mathcal{J}(\lambda_k).
\end{aligned}$$

The previous proposition is actually the proof of the following theorem

Theorem 2.1. *The problem (1.10) admits at least a solution in $\mathcal{U}_{ad}$.*

3. The proposed algorithm and numerical approximation.

3.1. Algorithm. In this section, we present the proposed algorithm that allows to approximate the solution of the our problem (1.10). The algorithm based on the projected gradient method and the numerical approximation of the state and adjoint problems. The basic idea of projection methods is for a suitable descent direction without bound constraints, then we project the new iteration onto the admissible set giving by the inequality constraints. So, to generate the our algorithm, we apply the Lagrange multiplier approach to give the optimality conditions of the proposed PDE constrained optimization problem [22]. We first consider the solution to the unconstrained problem, where no bound constraints on the control λ are present. We can write the Lagrangian function $\mathcal{L}$ associated with the problem:

$$\begin{aligned}\mathcal{L}(u,v,\lambda) = \mathcal{J}(\lambda) - \int_0^T\int_\Omega \partial_t u v dxdt - \int_0^T\int_\Omega \frac{\log^\gamma(1+|\nabla u(x)|)}{|\nabla u(x)|}\nabla u(x)\nabla v(x)dxdt \\ - \int_0^T\int_\Omega \lambda\left(u(x)-u_0\right)v(x)dxdt\end{aligned},$$

where v is the Lagrange multipliers.
Since, the control is considered with a box constraints, the optimality condition

$$\begin{aligned}\nabla_u\mathcal{L}(\bar{u},\bar{\lambda},v)u = 0 \quad \text{for all } u \\ \nabla_\lambda\mathcal{L}(\bar{u},\bar{\lambda},v)(\lambda-\bar{\lambda}) \geq 0 \quad \text{for all } \lambda\in\mathcal{U}_{ad},\end{aligned}$$

where $\bar{\lambda}$ is the optimal control with the corresponding state $\bar{u}$.
And $\mathcal{U}_{ad} = \left\{\lambda\in L^2(\Omega) : \lambda_a \leqslant \lambda(x) \leqslant \lambda_b \text{ a.e in } \Omega\right\}$ is the set of admissible controls.
The first equation leads to the following adjoint equation:

$$(\mathcal{AE})\begin{cases} -\dfrac{\partial v}{\partial t} + div\left(\dfrac{\gamma\log^{\gamma-1}(1+|\nabla u|)}{1+|\nabla u|}\nabla v\right) - \lambda v = 0, \quad on\ ]0,T[\times\Omega, \\ v(T,x) = u_0(x) - u(T,x), \quad on\ \ ]0,T[\times\partial\Omega, \\ u(0,x) = u_0(x).\end{cases} \tag{3.1}$$

Evaluation of the variational inequality for the partial derivative with respect to λ of $\mathcal{L}$ yields

$$\nabla_\lambda\mathcal{L}(\bar{u},\bar{\lambda},v)(\lambda-\bar{\lambda}) = \alpha\int_\Omega\bar{\lambda}(\lambda-\bar{\lambda})dx - \int_0^T\int_\Omega(\bar{u}(t,x)-u_0)v(t,x)(\lambda-\bar{\lambda})dxdt \geq 0 \text{ for all } \lambda\in\mathcal{U}_{ad}$$

We conclude that

$$\left(\alpha\bar{\lambda} - \int_0^T(\bar{u}(t)-u_0)v(t)dt, \lambda-\bar{\lambda}\right) \geq 0 \text{ for all } \lambda\in\mathcal{U}_{ad}.$$

Then, for $\alpha > 0$, the optimal control satisfies the following projection relation [22]:

$$\bar{\lambda} = \mathbb{P}_{[\lambda_a,\lambda_b]}\left\{\frac{\int_0^T(\bar{u}(t)-u_0)v(t)dt}{\alpha}\right\}$$

Where, for real numbers $a \leq b$, $\mathbb{P}_{[a,b]}$ denotes the projection onto $[a,b]$,

$$\mathbb{P}_{[a,b]}(x) := \max\{a, \min\{b, x\}\}$$

Finally, the projected descent algorithm for the problem (1.10) is given through the following algorithm 1:

Algorithm 1 Projected descent method.

1. Choose u_0 be a noisy image, $\lambda_0 \in \mathcal{U}_{ad}$, $\alpha > 0$ and set $n = 0$.
2. **repeat**
3. The state (1.11) and adjoint (3.1) equations.
4. Compute a descent direction d_n by
$$d_n = -\left(\alpha\lambda_n - \int_0^T (u_n - u_0)v_n dt\right)$$
5. Determine the optimal step size α_n.
6. Set
$$\lambda_{n+1} = \mathbb{P}_{[\lambda_a,\lambda_b]}(\lambda_n + \alpha_n d_n) \quad and\ n = n+1$$
7. **until** stopping criteria

3.2. Numerical results. In this section, we will focus on the presentation of the most significant results that demonstrated the effectiveness of the proposed restricted POE model compared to some competing settlement methods.

Our results are compared with some competitive denoising methods, including the TV model [14], the TGV model [5] and the denoising PDE where the parameter λ is a scalar.

Peak Signal to Noise Ratio (PSNR) (ratio of the maximum value of the image to the mean quadratic error between the original image and (SSIM) (computed over multiple viewports of a given image) are intended to measure the quality of the resulting images, which are defined as follows

$$\texttt{PSNR} = 10\log_{10}\left(\frac{255^2}{\texttt{MSE}}\right), \tag{3.2}$$

with MSE is the mean square error resulting in the following

$$\texttt{MSE} = \frac{1}{nm}\sum_{i=1}^{m}\sum_{j=1}^{n}(u(i,j) - v(i,j))^2,$$

where u be the noise-free image of size $m \times n$ and v the restored image.

$$\texttt{SSIM}(\texttt{u},\texttt{v}) = \frac{(2\sigma_u\sigma_v + r_2)\,(2\mu_u\mu_v + r_1)\,(2\,\mathrm{cov}\,uv + r3)}{(\mu_u^2 + \mu_v^2 + r_1)\,(\sigma_u^2 + \sigma_v^2 + r_2)\,(\sigma_u\sigma_v + r_3)} \tag{3.3}$$

with cov_{uv} is covariance and $r_1 = (m_1 l)^2, r_2 = (m_2 l)^2$ are two stabilizing constants; and l the dynamics of the pixel values. μ_u and μ_v; σ_u^2 and σ_v^2 are mean; variance of u and v respectively.



FIGURE 1. Test images for comparison experiments.

Using different regularizers; classical method (CL) [1], TV model [14] and TGV model [5], the figure (2) show the evolution of PSNR and SSIM of the reconstruction results up to 120 iterations (with $\sigma_{noise} = 30$). We notice that the evolution of PSNR and SSIM associated with our approach is higher than the other methods. This demonstrates the effectiveness of the proposed PDE.

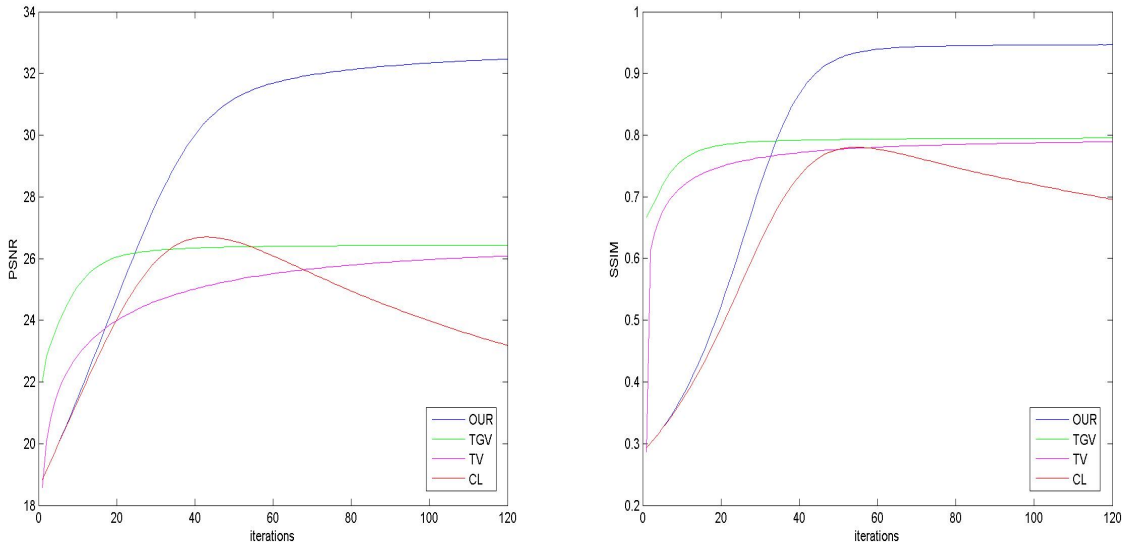


FIGURE 2. The variation of the PSNR and SSIM values (where $\sigma_{noise} = 30$) compared to the number of iterations for various regularizers (Cameraman image).

Figures 2-7 present the validation tests of our algorithm and the obtaining of the restoration of images noisy by different levels of noise ($\sigma_{noise} = 30$ and $\sigma_{noise} = 40$). From the obtained results, shows the performance of the proposed algorithm to solve the problem of image denoising.

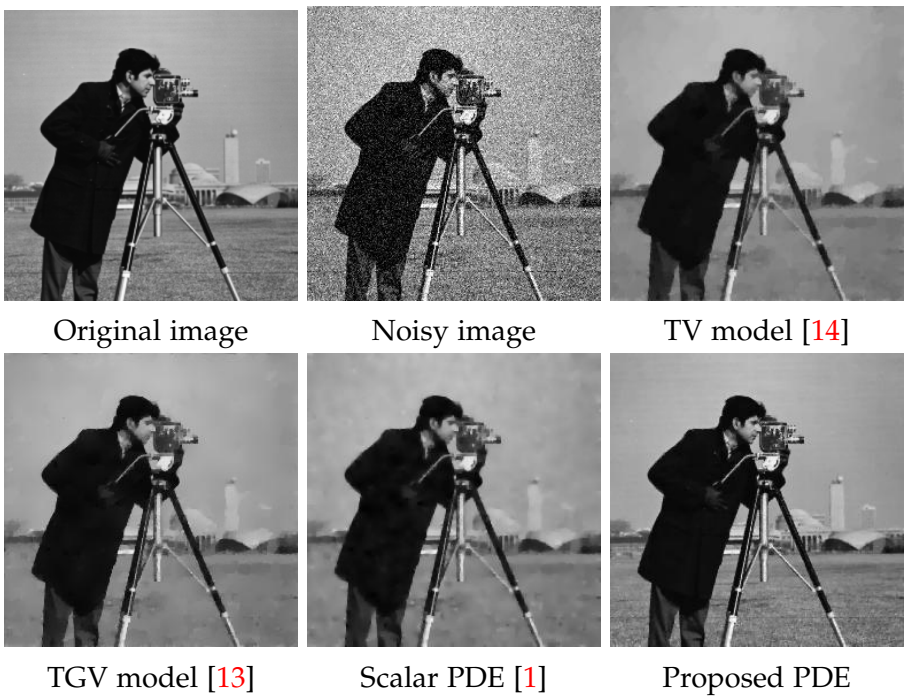


FIGURE 3. Comparisons of different denoising methods (Cameraman image), with $\sigma_{noise} = 30$.

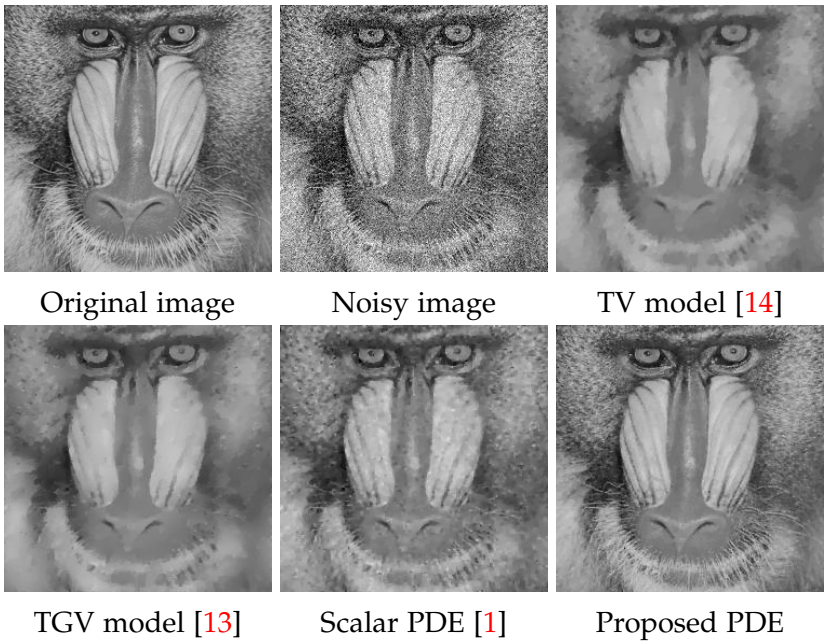


FIGURE 4. Comparisons of different denoising methods (Baboon image), with $\sigma_{noise} = 30$.

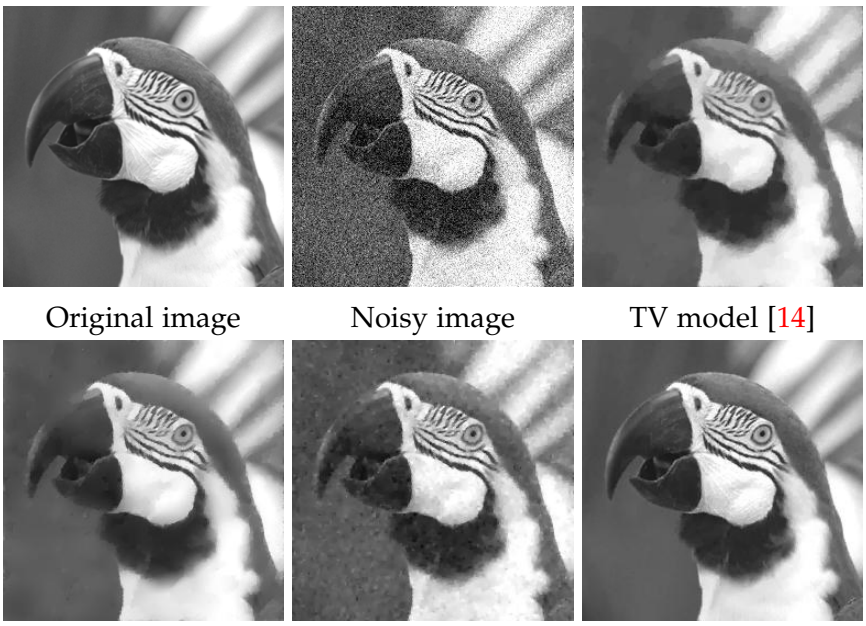


FIGURE 5. Comparisons of different denoising methods (Parrots image), with $\sigma_{noise} = 30$.

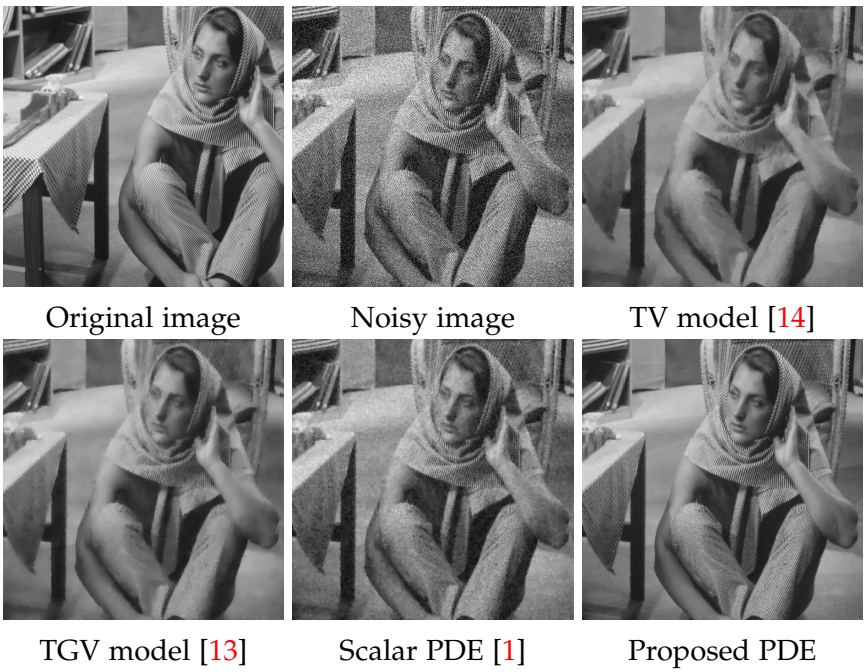


FIGURE 6. Comparisons of different denoising methods (Barbara image), with $\sigma_{noise} = 30$.

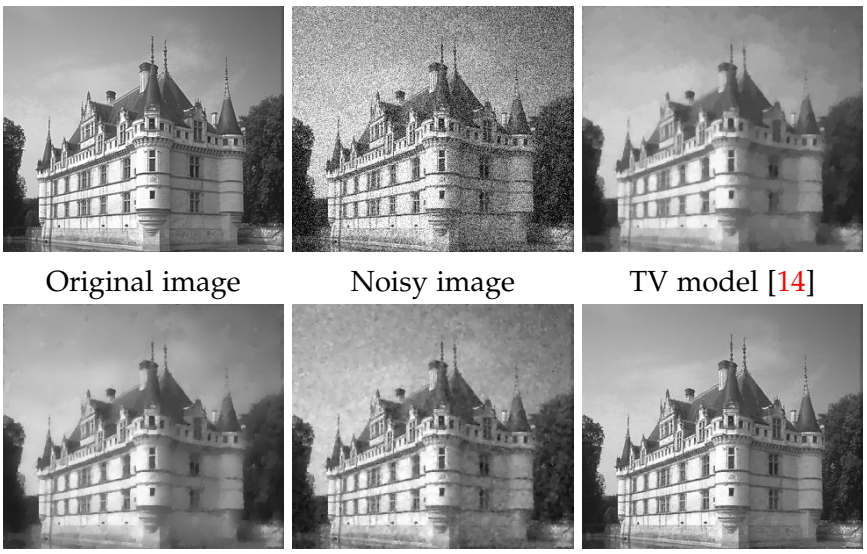


FIGURE 7. Comparisons of different denoising methods (Castle image), with $\sigma_{noise} = 30$.

For a choice of an additive white Gaussian noise of level $\sigma_{noise} = 30$ and $\sigma_{noise} = 40$, the two Tables 1 and 2 illustrate the different values of PSNR and SSIM respectively associated with the different approaches (TV model [14], TGV model [13], scalar EDP [1] and our approach). It is clear that the values of either PSNR or SSIM are higher than the other methods.

Image		PSNR				
	Noise	Noisy	TV [20]	TGV[5]	Scalar PDE [1]	Our propose
Cameraman	30	18.552	26.085	26.428	26.788	**32.503**
	40	16.058	25.365	25.495	25.231	**31.248**
Baboon	30	18.603	23.480	23.543	24.414	**29.550**
	40	16.122	23.421	23.498	23.455	**28.826**
Parrots	30	18.612	27.790	28.205	28.289	**34.796**
	40	16.047	26.887	27.012	27.042	**33.909**
Barbara	30	18.567	24.381	24.507	25.018	**30.681**
	40	16.117	24.146	24.198	23.998	**29.825**
Castle	30	18.574	24.466	24.750	25.398	**31.172**
	40	16.029	24.013	24.218	24.040	**29.937**

TABLE 1. The table of **PSNR** values.

Image		SSIM				
	Noise	Noisy	TV [20]	TGV[5]	Scalar PDE [1]	Our propose
Cameraman	30	0.287	0.796	0.800	0.780	**0.947**
	40	0.220	0.705	0.716	0.743	**0.940**
Baboon	30	0.426	0.512	0.519	0.643	**0.897**
	40	0.316	0.500	0.540	0.570	**0.883**
Parrots	30	0.253	0.844	0.858	0.844	**0.960**
	40	0.188	0.800	0.793	0.824	**0.957**
Barbara	30	0.598	0.797	0.805	0.803	**0.963**
	40	0.496	0.772	0.792	0.765	**0.956**
Castle	30	0.339	0.764	0.776	0.768	**0.950**
	40	0.263	0.718	0.745	0.723	**0.941**

TABLE 2. The table of **SSIM** values.

4. Conclusion

In this paper, we have proposed a projected descent algorithmic approach to solve optimization problems with PDE constraints arising in image denoising. The existence of a solution for the proposed optimization problem is proved and the numerical approximations demonstrate quantitatively and visually the efficiency of this PDE compared to some few denoising approaches known in the literature.

References

[1] Aboulaich, Rajae, Driss Meskine, and Ali Souissi. "New diffusion models in image processing." Computers & Mathematics with Applications 56.4 (2008): 874-882.
[2] Afraites, L., Atlas, A., Karami, F., & Meskine, D. (2016). Some class of parabolic systems applied to image processing. Discrete & Continuous Dynamical Systems-B, 21(6), 1671.
[3] Afraites, L., Hadri, A., Laghrib, A., & Nachaoui, M. (2021). A weighted parameter identification PDE-constrained optimization for inverse image denoising problem. The Visual Computer, 1-16.
[4] Bredies, Kristian, Karl Kunisch, and Thomas Pock. "Total generalized variation." SIAM Journal on Imaging Sciences 3.3 (2010): 492-526.
[5] Bergounioux, Maïtine, and Loic Piffet. "A second-order model for image denoising." Set-Valued and Variational Analysis 18.3 (2010): 277-306.
[6] Bergounioux, M., & Piffet, L. (2010). A second-order model for image denoising. Set-Valued and Variational Analysis, 18(3), 277-306.
[7] Catté, F., Lions, P. L., Morel, J. M., & Coll, T. (1992). Image selective smoothing and edge detection by nonlinear diffusion. SIAM Journal on Numerical analysis, 29(1), 182-193.
[8] J. C. De los Reyes, C.-B. Sch onlieb, T. Valkonen, Bilevel parameter learning for higher-order total variation regularisation models, Journal of Mathematical Imaging and Vision 57 (1) (2017) 1-25.

[9] Elmahi, A., and D. Meskine. "Strongly nonlinear parabolic equations with natural growth terms in Orlicz spaces." Nonlinear Analysis: Theory, Methods & Applications 60.1 (2005): 1-35.
[10] Elmahi, A., and D. Meskine. "Parabolic equations in Orlicz spaces." Journal of the London Mathematical Society 72.2 (2005): 410-428.
[11] El Mourabit, I., El Rhabi, M., Hakim, A., Laghrib, A., & Moreau, E. (2017). A new denoising model for multi-frame super-resolution image reconstruction. Signal Processinknog, 132, 51-65.
[12] S. Farsiu, D. Robinson, M. Elad, P. Milanfar, Advances and challenges in super-resolution, Interna-tional Journal of Imaging Systems and Technology 14 (2) (2004) 47-57.
[13] Michael Hintermüller, Kostas Papafitsoros, Carlos N. Rautenberg & Hongpeng Sun (2022) Dualization and Automatic Distributed Parameter Selection of Total Generalized Variation via Bilevel Optimization, Numerical Functional Analysis and Optimization, 43:8, 887-932.
[14] Hintermüller, Michael, and Carlos N. Rautenberg. "Optimal selection of the regularization function in a weighted total variation model. Part I: Modelling and theory." Journal of Mathematical Imaging and Vision 59.3 (2017): 498-514.
[15] M. Hinterm uller, C. N. Rautenberg, T. Wu, A. Langer, Optimal selection of the regularization function in a weighted total variation model. part ii: Algorithm, its analysis and numerical tests, Journal of Mathematical Imaging and Vision 59 (3) (2017) 515-533.
[16] JAIN, Anil K. Fundamentals of digital image processing. Prentice-Hall, Inc., 1989.
[17] A. Lanza, S. Morigi, F. Sgallari, Constrained TV_p-l_2 model for image restoration, Journal of Scientific. Computing 68 (1) (2016) 64-91.
[18] Nocedal, Jorge, and Stephen J. Wright, eds. Numerical optimization. New York, NY: Springer New York, 1999.
[19] Perona, P., & Malik, J. (1990). Scale-space and edge detection using anisotropic diffusion. IEEE Transactions on pattern analysis and machine intelligence, 12(7), 629-639.
[20] Rudin, Leonid I., Stanley Osher, and Emad Fatemi. "Nonlinear total variation based noise removal algorithms."Physica D: nonlinear phenomena 60.1-4 (1992): 259-268.
[21] Lv, X. G., Song, Y. Z., Wang, S. X., & Le, J. (2013). Image restoration with a high-order total variation minimization method. Applied Mathematical Modelling, 37(16-17), 8210-8224.
[22] Tröltzsch, Fredi. Optimal control of partial differential equations: theory, methods, and applications. Vol. 112. American Mathematical Soc., 2010.
[23] C. Van Chung, J. De los Reyes, C. Sch onlieb, Learning optimal spatially-dependent regularization parameters in total variation image denoising, Inverse Problems 33 (7) (2017) 074005.
[24] Yaroslavsky, L. P. (2012). Digital picture processing: an introduction (Vol. 9). Springer Science & Business Media.
[25] Zhang, J., & Chen, K. (2015). A total fractional-order variation model for image restoration with nonhomogeneous boundary conditions and its numerical solution. SIAM Journal on Imaging Sciences, 8(4), 2487-2518.